Journal of Nuclear Materials 382 (2008) 203–209

Contents lists available at ScienceDirect

Journal of Nuclear Materials

journal homepage: www.elsevier.com/locate/jnucmat

Localized deformation and IASCC initiation in austenitic stainless steels

Z. Jiao *, G.S. Was

University of Michigan, Department of Nuclear Engineering and Radiological Sciences, Ann Arbor, MI 48109, United States

A B S T R A C T

Localized deformation may play a key role in the underlying mechanism of irradiation assisted stress corrosion cracking (IASCC) in light water reactor core components. In this study, four austenitic alloys, 18Cr8Ni, 15Cr12Ni, 13Cr15Ni and 21Cr32Ni, with different stacking fault energies were irradiated to 1 and 5 dpa at 360 °C using 3.2 MeV protons. Interrupted constant extension rate tensile (CERT) tests were conducted in a simulated BWR environment to determine IASCC susceptibility. In order to characterize the localized deformation in slip channels and grain boundaries, parallel CERT experiments were also performed in an argon atmosphere. Results show that the IASCC susceptibility of the tested alloys increases with increasing irradiation dose and decreasing stacking fault energy. IASCC tends to initiate at locations where slip channels intersect grain boundaries. Localized deformation in the form of grain boundary sliding due to the interaction of slip channels and grain boundaries is likely the primary cause of the observed cracking initiation.

1. Introduction

Irradiation assisted stress corrosion cracking (IASCC) is the primary form of core component cracking in boiling water reactors (BWR). An understanding of the mechanism of IASCC is required in order to provide guidance for the development of mitigation strategies. However, IASCC is a very complex phenomenon. It is known to be affected by both the water environment and the irradiated microstructure [1]. As for the materials, changes due to irradiation, such as microstructure, grain boundary chemistry and hardening, all follow a similar dose dependence [2], which make the IASCC mechanism even more difficult to understand.

The composition change at grain boundaries, especially the depletion of Cr, is generally assumed to be the primary cause of IASCC. However, post-irradiation annealing (PIA) experiments on proton-irradiated alloy 304 [3] suggest that Cr depletion is not the primary determinator for IASCC susceptibility. Jacobs [4] also reported that the depletion of Cr did not appear to be the causative factor in IASCC in neutron-irradiated 304SS. A more comprehensive study [5] of nine model austenitic alloys suggests that radiation-induced segregation (RIS) alone does not control IASCC susceptibility. The determinative role of RIS in IASCC is, therefore, challenged.

On the other hand, a few experiments suggest that localized deformation may play an important role in IASCC. For instance, deformation steps were frequently observed on the fracture surface of irradiated austenitic stainless steels under simulated BWR conditions [6]. Surface slip steps were also found to be much greater on samples that cracked [7]. Onchi et al. [8] reported that intergranular facets were associated with various patterns of linear features/steps in thermally sensitized 304 stainless steel and that crack initiation sites tended to be related to the deformation bands [9]. Previous studies by the authors [10,11] also suggested that localized deformation, which can be enhanced by low stacking fault energy (SFE) and irradiation, was a potential contributor to IASCC.

The objective of this work is to understand the contribution of localized deformation to the underlying mechanism of IASCC by examining IASCC initiation and localized deformation in proton-irradiated austenitic stainless steels after constant extension rate tensile (CERT) tests in simulated BWR environment and argon atmosphere.

2. Experimental

2.1. Alloy selection, sample preparation and proton irradiations

Four austenitic alloys with nominal compositions of 18Cr8Ni, 15Cr12Ni, 13Cr15Ni and 21Cr32Ni were selected in this study. The compositions of these alloys are listed in Table 1. Alloys were used in the solution-annealed condition without any additional processing. After the tensile samples (dimensions are shown in Fig. 1) were fabricated using electric discharging machine, the surfaces were grounded using SiC paper to a final finish of #4000 grit. The samples were then electropolished in a 10% perchloric acid, 90% methanol solution at −40° to get a mirror like surfaces prior to irradiation experiment.

* Corresponding author.
E-mail address: zjiao@umich.edu (Z. Jiao).

0022-3115/$ - see front matter © 2008 Elsevier B.V. All rights reserved.
doi:10.1016/j.jnucmat.2008.08.032

Table 1
Compositions (wt%) of selected alloys

Alloy	Fe	Cr	Ni	Mn	Si	P	C
18Cr8Ni	Bal.	18.30	8.50	1.38	0.65	0.03	0.04
15Cr12Ni	Bal.	15.76	12.04	0.98	0.10	<0.01	0.02
13Cr15Ni	Bal.	13.41	15.04	1.03	0.10	<0.01	0.02
21Cr32Ni	Bal.	20.73	31.16	0.94	0.10	0.014	0.014

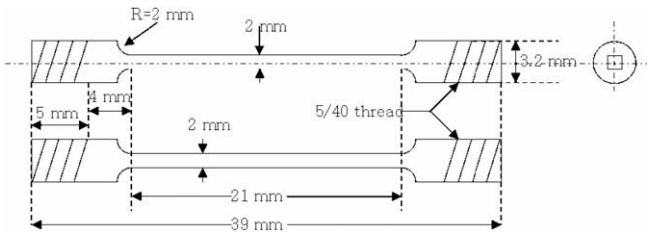

Fig. 1. Dimensions of the tested samples.

Irradiations of samples were performed using a specially designed stage connected to the General Ionex Tandetron accelerator at the Michigan Ion Beam Laboratory. Irradiations were conducted using 3.2 MeV protons at a dose rate of approximately 8.5×10^{-6} dpa/s (the experimental doses and dose rates are calculated using SRIM2003 [12]), resulting in a nearly uniform damage rate through the first 35 μm of the proton range (total ~40 μm). Two batches of samples were irradiated to 1.0 and 5.0 dpa, respectively. The sample temperature was maintained at 360 ± 10 °C for the duration of each irradiation. A more detailed description of the proton irradiation procedure can be found elsewhere [13].

2.2. Interrupted constant extension rate tensile (CERT) tests

Interrupted CERT tests were conducted under simulated BWR conditions to examine IASCC initiation. Water chemistry at the testing condition (288 °C, 0.2 μS/cm conductivity and 2 ppm O_2 content) was allowed to stabilize for at least one day prior to straining. Alloys were first strained to 1% plastic strain at a strain rate of 3.5×10^{-7} s^{-1}. The test was then interrupted and the samples were removed from the autoclave for scanning electron microscopy (SEM) examination of cracking on the gage section. If IASCC initiation was observed, no further straining was performed on the sample. Samples without cracks were then strained to the next strain level of 3% and the sample surfaces were once again examined for cracks. Samples showing no sign of cracks were further strained to the ultimate tensile stress (UTS) and the test was terminated. Because the characterization of the localized deformation requires a clean sample surface, parallel interrupted CERT tests were also performed in argon in a multiple-specimen test system at 288 °C using the same strain rate. The degree of localized deformation in alloys 15Cr12Ni and 21Cr32Ni was examined using atomic force microscopy (AFM) at two strain levels: 1% and 3%.

3. Results and discussion

3.1. SFE measurement

It is known that SFE of austenitic alloy varies with nickel and chromium compositions. SFE can be estimated using empirical equations such as the one proposed by Pickering [14]. However, as SFE may play a fundamental role in our study, it is necessary to obtain SFE experimentally. In an austenitic alloy, a perfect dislocation with Burgers vector $\mathbf{b} = 1/2\langle 1\,1\,0\rangle$ dissociates into two partial dislocations with Burgers vector $\mathbf{b} = 1/6\langle 1\,1\,2\rangle$ on $\{1\,1\,1\}$ planes. The spacing of the two dislocation partials at equilibrium is inversely proportional to the stacking fault energy [15]. Therefore, the SFEs can be obtained by measuring the spacing between dislocation partials. This work was done on a JOEL 2010F transmission electron microscopy (TEM) operating at 200 V at the University of Michigan Electron Microbeam Analysis Laboratory (EMAL). Fig. 2 shows an example of a dissociated dislocation imaged using weak beam dark field technique in alloy 18Cr8Ni. The separation between the two partial dislocations is clearly shown in this figure. Only isolated dislocations which are at least 100 nm away from others were selected for measurement. About 15 measurements were made on each alloy. The measured SFEs together with those predicted using Pickering's equation are shown in Fig. 3. The measured values are always smaller than the predicted ones. However, they follow the same trend, indicating that the composition-dependence of the SFE correlation in Pickering's equation is generally valid. The SFE increases in the order of 18Cr8Ni, 15Cr12Ni,

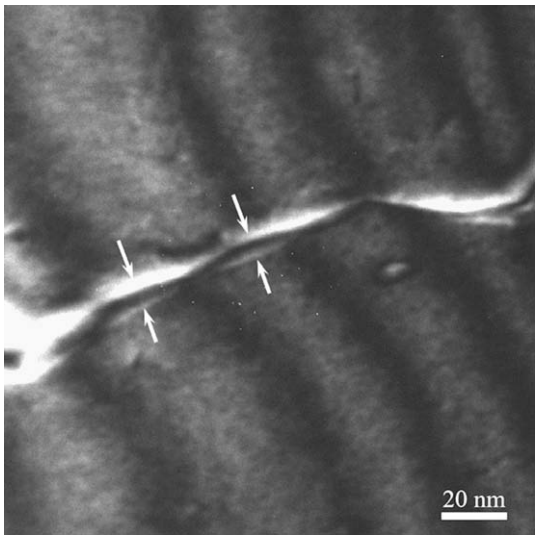

Fig. 2. A dissociated dislocation imaged using $g/3g$ weak beam dark field TEM technique in alloy 18Cr8Ni. Imaging conditions: $B = 1\,1\,0$ and $g = -1\,1\,1$. Arrows show the separation between partial dislocations.

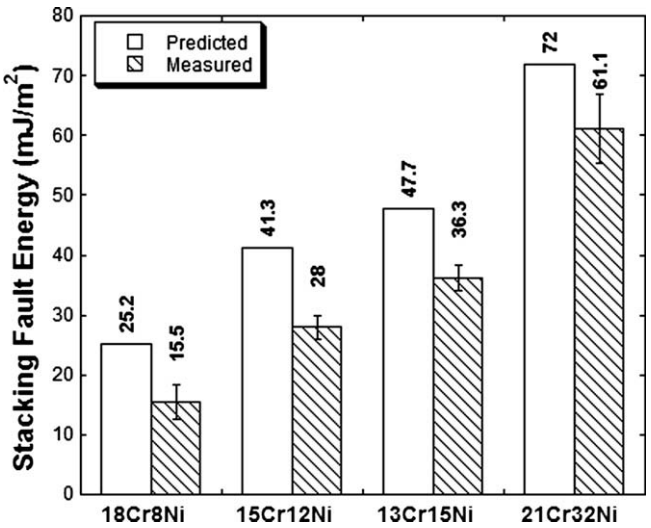

Fig. 3. Stacking fault energy predicted using Pickering's equation [14] and measured in this study.

13Cr15Ni and 21Cr32Ni. Increasing Ni content generally results in an alloy with higher SFE.

3.2. IASCC initiation

Interrupted CERT tests were performed on the four alloys at doses of 1 and 5 dpa under simulated BWR conditions. The surfaces were examined using SEM after each strain interval. At 5 dpa, cracks were observed in alloys 18Cr8Ni (Fig. 4(a)) and 15Cr12Ni (Fig. 4(b)), the two lowest SFE alloys, at 1% strain. However, 15 grain boundaries cracked in alloy 18Cr8Ni while only five grain boundaries were found to be associated with crack initiation in alloy 15Cr12Ni in a total examined area of 2 mm × 10 mm. Alloy 13Cr15Ni started to show cracks at 3% strain (Fig. 4(c)). No cracks were observed in alloy 21Cr32Ni even after strained to UTS (~27% total strain). At 1 dpa, cracks were only observed in alloy 18Cr8Ni starting at 3% strain (Fig. 4(d)). The IASCC susceptibility in terms of the inverse of strain-to-failure as a function of stacking fault energy and irradiation dose is shown in Fig. 5. Alloy 18Cr8Ni with the lowest stacking fault energy cracks at both low and high doses. However, alloy 21Cr32Ni with the highest stacking fault energy is resistant to cracking regardless of doses. The two moderate SFE alloys, 15Cr12Ni and 13Cr15Ni, only crack at 5 dpa. Nevertheless, alloy 13Cr15Ni with higher SFE cracks at a higher strain level. The CERT test results show that low stacking fault energy and high irradiation dose promote intergranular stress corrosion cracking. This is consistent with a previous study [10].

Crack initiation sites were carefully examined in alloy 15Cr12Ni at the condition of 5 dpa and 1% strain. Cracks were observed to initiate preferably at locations where a slip line intersected a grain boundary. A total of six crack initiation sites were found in alloy 15Cr12Ni and all of them can be linked to the interaction of slip lines with grain boundaries. One example of crack initiation sites is shown in Fig. 6. Very likely, the initiation of cracks was the result of grain boundary deformation which was caused by the impingement of slip lines as indicated by small arrows in the inserts. Similar crack initiation sites were also observed in alloy 13Cr15Ni. All of the cracks observed in alloy 18Cr8Ni (total of 10) were associated with slip lines. It is authors' belief that at the very beginning of the crack initiation stage, localized deformation as the result of the interaction of slip lines with grain boundaries plays a crucial role. The quantitative information of localized deformation is usually difficult to be obtained from samples tested under BWR conditions due to surface corrosions. Therefore, it is necessary to conduct parallel experiments in argon in favor of a clean sample surface.

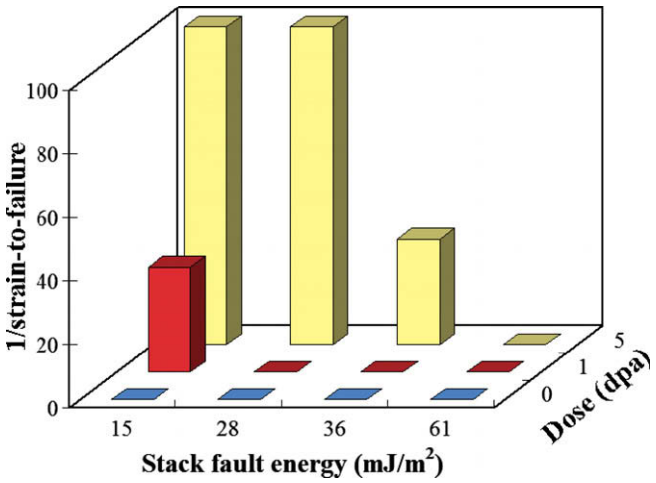

Fig. 5. Inverse of strain-to-failure as a function of stacking fault energy and irradiation dose.

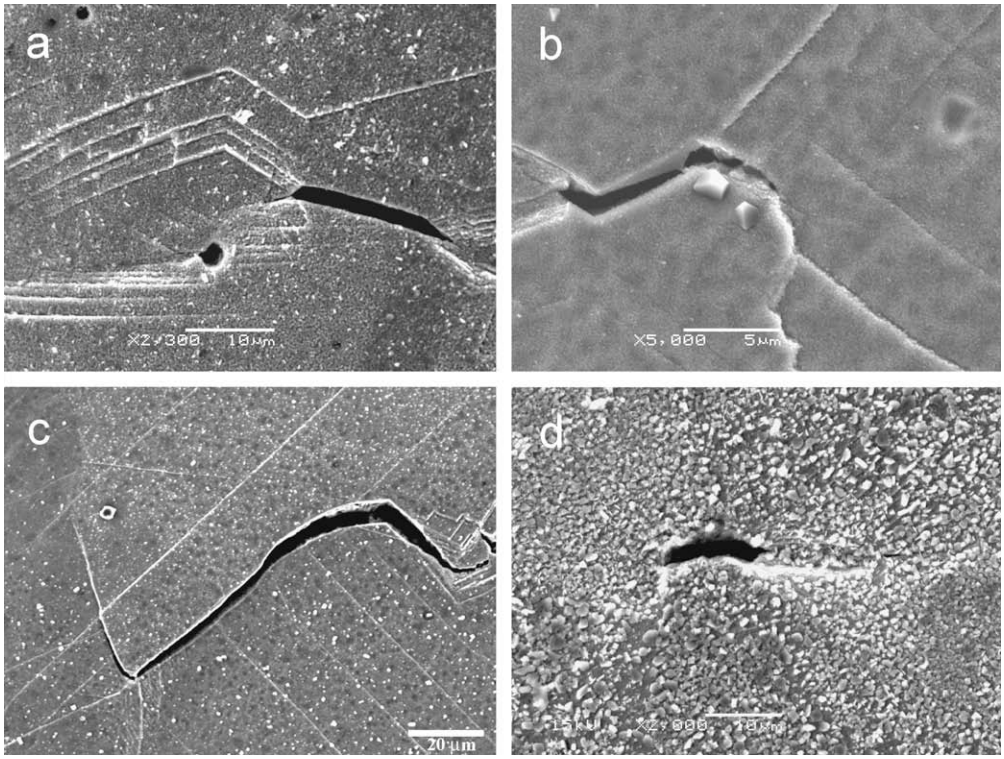

Fig. 4. Cracks in proton-irradiated austenitic stainless steels strained in simulated BWR environment: (a) 18Cr8Ni at 5 dpa and 1% strain, (b) 15Cr12Ni at 5 dpa and 1% strain, (c) 13Cr15Ni at 5 dpa and 3% strain and (d) 18Cr8Ni at 1 dpa and 3% strain.

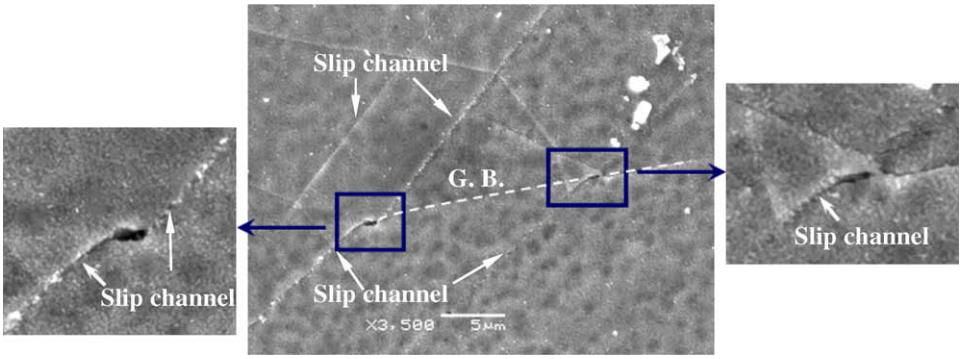

Fig. 6. Crack initiation in proton-irradiated 15Cr12Ni strained to 1% in simulated BWR environment. The position of the grain boundary is highlighted by dashed line. The slip lines are indicated by small arrows in the inserts.

3.3. Localized deformation

Dislocation channeling is normally the main deformation mode in irradiated austenitic stainless steels [16]. During deformation, the majority of dislocation activities occur in dislocation channels. As a result, slip lines on the surface of irradiated alloys are much fewer in quantity but much more 'visible' under SEM than those in unirradiated alloys. Since slip lines in irradiated alloys are the results of dislocation slip in channels, they are referred to slip channels thereafter in this article. Fig. 7 shows the typical morphologies of slip channels observed on the surface of proton-irradiated austenitic alloys strained in argon at 288 °C. A notable feature of slip channels in both alloys strained to 1% is their inhomogeneity. First, the spacing between slip lines varies from one grain to another and even within the same grain. For instance, the spacing between slip lines in Fig. 7(b) can be as large as 30 μm and as low as 1 μm. Secondly, the amount of deformation in slip channels fluctuates. Some slip channels as indicated by arrows in Fig. 7(a) and (b) obviously have much greater deformation than others. Within the same grain, the height of slip channels in alloy 21Cr32Ni at 1 dpa and 1% strain ranges from 34 to 245 nm. As the samples are strained further to 3%, both channel height and spacing tend to be more homogenous (Fig. 7(c)). The largest spacing between channels in Fig. 7(c) is about 15 μm.

Experimental observations [17,18] suggest that dislocations originating from grain boundaries and other stress concentrators are responsible for defect-free channels. General grain boundaries have many irregular sites such as micro-scale ledges that, under certain stress, can emit lattice dislocations [19]. In the unirradiated alloy in the annealed condition, the dislocation density is very low. At the beginning of plastic deformation, the emitted lattice dislocations can glide easily once the applied stress reaches the critical resolved shear stress. However, in an irradiated alloy, the simultaneous glide of an array of dislocations is required to annihilate the defect obstacles and initiate defect-free dislocation channels [20]. Thus, even within the same grain boundary, only certain irregular sites with the capability to emit large number of dislocations can initiate dislocation channels. Since most of the applied deformation goes into these channels, the amount of deformation in the channels can be very large. Initiation of channels from other irregular sites is suppressed because of insufficient number of dislocations emitted. As a result, when the applied strain is small (~1%), the slip channels are inhomogeneous both in channel height and spacing. When the samples are strained further, more irregular sites meet the requirement and initiate dislocation channels. Therefore, the density of slip channels at a higher strain increases, resulting in greater homogeneity.

The amount of deformation in slip channels was characterized using AFM for alloys 15Cr12Ni and 21Cr32Ni. As shown in Fig. 8, the average step height varies with alloy, irradiation dose and strain level. The amount of deformation in slip channels is much higher in low SFE alloy 15Cr12Ni than high SFE alloy 21Cr32Ni for the same irradiation dose and strain. Higher dose results in a higher amount of deformation in slip channels for the same alloy. Also for the same irradiation dose and alloy, larger strain results in larger deformation in channels. These results are expected as low SFE and high irradiation dose promote planar slip and are consistent with our previous study [10]. Since the amount of deformation in slip channels is affected by local stress states, grain orientations, etc., a significant body of data will be required to support this observation in a statistically meaningful fashion.

Since IASCC is typically in the form of intergranular cracking, it is more of interest to examine localized deformation at grain boundaries. In general, grain boundary deformation includes grain boundary sliding and migration. Grain boundary migration is a diffusionally accommodated process and mostly occurs at high temperatures. However, grain boundary sliding can be either diffusionally accommodated or achieved by glide of grain boundary dislocations. Furthermore, grain boundary sliding can be

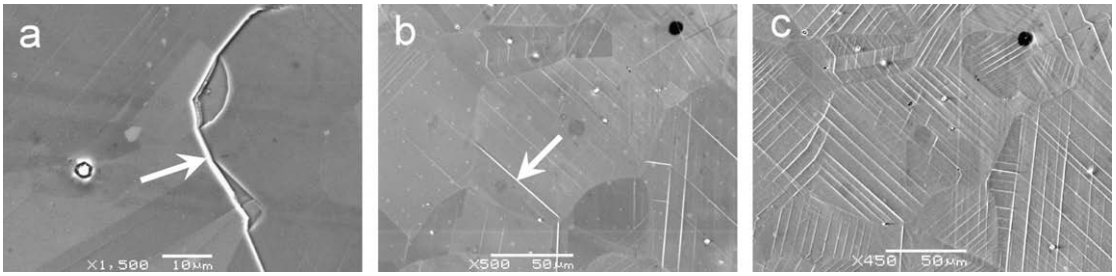

Fig. 7. Morphologies of slip channels on the surface of irradiated samples strained in argon at 288 °C: (a) 15Cr12Ni at 5 dpa and 1%, (b) 21Cr32Ni at 1 dpa and 1% and (c) 21Cr32Ni at 1 dpa and 3%.

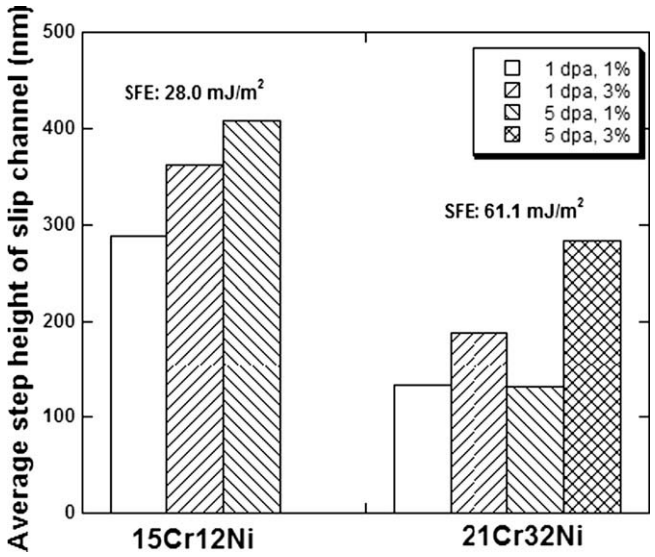

Fig. 8. Average step height in the slip channel in alloys 15Cr12Ni (SFE, 28.0 mJ/m^2) and 21Cr32Ni (SFE, 61.1 mJ/m^2) at two doses and strain levels.

significantly enhanced by the impingement of lattice dislocations on the grain boundary [21,22].

Fig. 9(a) is a surface plot containing a grain boundary obtained by AFM of 15Cr12Ni irradiated to 5 dpa and strained to 1%. A schematic of the plot is shown in Fig. 9(b). The grain boundary plane is indicated by arrows in both figures. Grain boundary sliding is clearly shown as the grain on the left of the boundary plane is displaced nearly vertically relative to the one on the right. The amount of displacement caused by sliding was measured to be ~380 nm. The sliding is likely caused by the interaction of the large slip channel (the boldest line in Fig. 9(b)) with the grain boundary. However, among all eight grain boundaries examined by AFM in high SFE alloy 21Cr32Ni, no grain boundary sliding is observed. Fig. 9(c) shows an example of AFM scan of a grain boundary in alloy 21Cr32Ni. The deformation is not confined to the grain boundary plane (dashed line in Fig. 9(c)) following irradiation to 1 dpa and straining to 3%. Instead, the deformation is distributed in a relatively large area containing the grain boundary (light color in Fig. 9(c)). Grain boundary sliding is termed 'planar' deformation because the deformation is localized in the grain boundary plane. It commonly occurs in low SFE alloy 15Cr12Ni irradiated to 5 dpa. 'Non-planar' deformation, which occurs in a relatively large area around grain boundaries, is widely observed in high SFE alloy 21Cr32Ni.

Grain boundary sliding is known to occur by the motion of grain boundary dislocations rather than by instantaneous shear of the entire boundary [21]. When a newly initiated dislocation channel intersects a grain boundary, it results in a pile-up of dislocations. When a higher stress is applied on the sample, more dislocations will join the dislocation queue. At a certain point, the leading dislocation will merge into the grain boundary. It becomes an extrinsic grain boundary dislocation (EGBD) and further dissociates into grain boundary dislocations. As more lattice dislocations under stress 'squeeze' into the grain boundary, the stress on the grain boundary dislocations will be high enough to cause the dislocations to glide. The glide of dislocations in the grain boundary results in grain boundary sliding. It is noteworthy that grain boundary sliding is very likely to be localized to a small region of the grain boundary close to the intersection with the channel. Localized grain boundary sliding is probably the cause of the formation of deformation ledges near slip channel – grain boundary intersections in Fig. 10. For the same reasoning, the crack initiation sites in Fig. 6 may be linked to localized grain boundary sliding. It has been hypothesized [23] that grain boundary deformation, especially grain boundary sliding, is the major contributor to IASCC. This hypothesis is supported by the observations in this study.

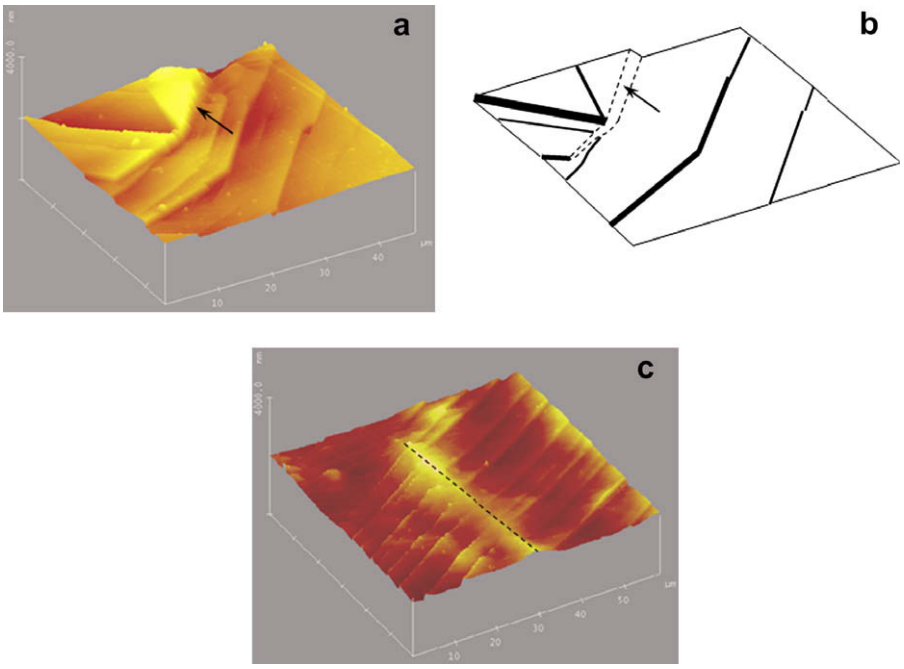

Fig. 9. Deformation at grain boundaries as characterized by AFM: (a) a surface plot in 15Cr12Ni at 5 dpa and 1% strain; (b) a schematic of the plot in (a); (c) a surface plot in 21Cr32Ni at 1 dpa and 3% strain. Arrows in (a) and (b) show the grain boundary deformation in alloy 15Cr12Ni. The amount of 'planar' deformation at the grain boundary caused by grain boundary sliding is bounded by dashed line in (b). The bold lines in (b) represent slip channels in (a). The dashed line in (c) indicates the position of the grain boundary in alloy 21Cr32Ni. Light color surrounding the dashed line is the sign of the broadened deformation in the grain boundary area.

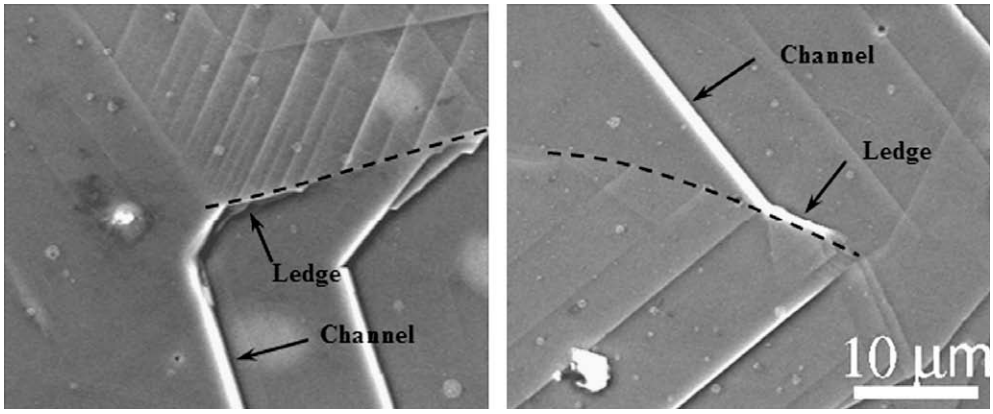

Fig. 10. Ledge formation due to dislocation channel and grain boundary interaction in proton-irradiated 15Cr12Ni strained to 1% in argon at 288 °C. The position of the grain boundary is indicated by a dashed line.

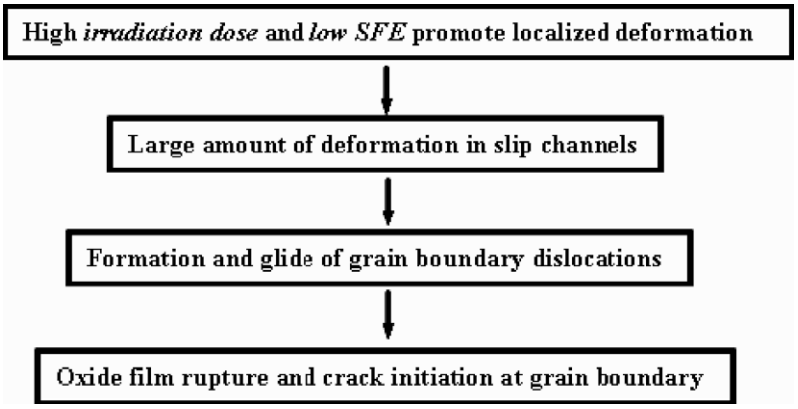

Fig. 11. Contribution of localized deformation to IASCC initiation.

3.4. Contribution of localized deformation to IASCC initiation

The contribution of localized deformation to IASCC initiation can be summarized in Fig. 11. Localized deformation in slip channels is enhanced by low SFE and high irradiation dose. As mentioned earlier, the large amount of localized deformation in dislocation channels may result in the formation and glide of grain boundary dislocations. The glide of grain boundary dislocations causes localized grain boundary sliding near the slip channel – grain boundary intersection. When this occurs on the samples tested under BWR conditions, localized grain boundary sliding may reach to the surface and rupture the oxide film above the grain boundary and IASCC initiates. In contrast, in a high SFE alloy with a low irradiation dose, the deformation caused by dislocation channels is distributed in a large area around the grain boundary. A significant amount of grain boundary dislocation activities is, therefore, not expected.

The contribution of localized deformation to IASCC has been discussed in detail in [23]. However, like most of other contributors to IASCC, localized deformation alone may not cause intergranular cracking. This is why for the same amount of deformation and irradiation dose, cracks were not observed in alloy 15Cr12Ni tested in argon atmosphere. Both corrosion and deformation at grain boundary are important in understanding the mechanism of IASCC. Water chemistry and RIS at grain boundary would contribute to the corrosion part of IASCC while localized grain boundary sliding would contribute to the deformation part. For different environment, the susceptibility to IASCC may differ even with the same amount of grain boundary deformation.

4. Conclusions

The IASCC susceptibility of the studied alloys increases with increasing irradiation dose and decreasing stacking fault energy when tested in a simulated BWR environment. Alloy 18Cr8Ni is susceptible to cracking at both 1 and 5 dpa. Alloys 15Cr12Ni and 13Cr15Ni with moderate SFEs are resistant to cracking at 1 dpa but are susceptible to cracking at 5 dpa. Alloy 13Cr15Ni with a higher SFE requires a higher strain to crack than alloy 15Cr12Ni. Alloy 21Cr32Ni with the highest SFE shows remarkable cracking resistance.

Localized deformation was characterized in proton-irradiated austenitic alloys 15Cr12Ni and 21Cr32Ni at 1% and 3% strain. The slip channels in both alloys are inhomogeneous at 1% plastic strain. At a higher strain of 3%, slip channels become more homogeneous. The average step height in the channel is much smaller in high SFE alloy 21Cr32Ni. High irradiation dose results in larger step height. Localized grain boundary sliding was observed in low SFE alloy 15Cr12Ni irradiated to 5 dpa and strained to 1%. Non-planar deformation around grain boundaries was observed in high SFE alloy 21Cr32Ni.

IASCC was found to initiate at locations where a large slip channel intersects a grain boundary in simulated BWR environment.

IASCC initiation in studied alloys can be linked to the localized grain boundary sliding near the slip channel – grain boundary intersections. Localized deformation is a very likely contributor to IASCC.

Acknowledgements

The authors gratefully acknowledge Dr Ovidiu Toader for his assistance in conducting proton irradiations. The authors also acknowledge the facilities provided by the Michigan Ion Beam Laboratory and the Electron Microbeam Analysis Laboratory at University of Michigan. Support for this research was provided by the EPRI/CIR program and the Department of Energy (DOE) under contract DE-FG07-05ID14703.

References

[1] P.L. Andresen, F.P. Ford, S.M. Murphy, J.M. Perks, in: Proceedings of 4th International Symposium on Environmental Degradation of Materials in Nuclear Power Systems, Water Reactors NACE International, Houston, 1990, p. 1.
[2] G.S. Was, in: Proceedings of 11th International Conference on Environmental Degradation of Materials in Nuclear Power Systems, Water Reactors, American Nuclear Society, La Grange Park, IL, 2003, p. 965.
[3] J.T. Busby, G.S. Was, E.A. Kenik, J. Nucl. Mater. 302 (2002) 20.
[4] A.J. Jacobs, in: A.S. Kumar, D.S. Gelles, R.K. Nanstad, E.A. Little (Eds.), 16th International Symposium On Radiation on Materials, ASTM-STP 1175, ASTM, Philadelphia, 1993, p. 902.
[5] J.T. Busby, G.S. Was, in: Proceedings of 11th International Conference on Environmental Degradation of Materials in Nuclear Power Systems, Water Reactors, American Nuclear Society, La Grange Park, IL, 2003, p. 995.
[6] J.T. Busby, PhD Thesis, University of Michigan, 2001.
[7] M.C. Hash, J.T. Busby, G.S. Was, in: M.R. Grossbeck, T.R. Allen, R.G. Lott, A.S. Kumar (Eds.), Effects of Radiation on Materials: 21st International Symposium, ASTM STP 1447, American Society for Testing of Materials, West Conshohocken, PA, 2002.
[8] T. Onchi, K. Dohi, N. Soneda a, J.R. Cowan, R.J. Scowen, M.L. Castano, J. Nucl. Mater. 320 (2003) 194.
[9] T. Onchi, K. Dohi a, N. Soneda, Marta Navas, M.L. Castano, J. Nucl. Mater. 340 (2005) 219.
[10] Z. Jiao, J.T. Busby, R. Obata, G.S. Was, in: Proceedings of 12th International Conference on Degradation of Materials in Nuclear Power Systems, Water Reactors and Minerals, Springer, London, 2003.
[11] Z. Jiao, J.T. Busby, G.S. Was, J. Nucl. Mater. 361 (2007) 218.
[12] J.F. Ziegler, J.P. Biersack, SRIM 2003 Program, IBM Corporation, Yorktown, NY.
[13] G. Gupta, Z. Jiao, A.N. Ham, J.T. Busby, G.S. Was, J. Nucl. Mater. 351 (2006) 162.
[14] F.B. Pickering, in: Proceedings of the Conference on Stainless Steels 84, Gothenberg, Sweden, 1984, The Institute of Metals, London, 1985, p. 2.
[15] D. Hull, D.J. Bacon, Introduction to Dislocations, International Series on Materials Science and Technology, vol. 37, Pergamon, 1984. p. 98.
[16] K. Farrell, T.S. Byun, N. Hashimoto, J. Nucl. Mater. 335 (2004) 471.
[17] D.J. Edwards, B.N. Singh, J.B. Bilde-Sørensen, J. Nucl. Mater. 342 (2005) 164.
[18] I.M. Robertson, J. Robach, B. Wirth, A. Arsenlis, Material Research Society Symposium Proceedings, vol. 779, Materials Research Society, 2003.
[19] E.V. Esquivel, L.E. Murr, Mater. Sci. Eng. A 409 (2005) 13.
[20] T.S. Byun, N. Hashimoto, J. Nucl. Mater. 354 (2006) 123.
[21] G.R. Kegg, C.A.P. Horton, J.M. Silcock, Philos. Mag. 27 (1973) 1041.
[22] R.J. Kurtz, R.G. Hoagland, J.P. Hirth, Philos. Mag. A 79 (1999) 665.
[23] G.S. Was, B. Alexandreanu, J. Busby, Advances in Fracture and Failure Prevention, Trans Tech Publications Ltd., Switzerland, 2004. p. 885.